

# Fully Printed Inverters using Metal-Oxide Semiconductor and Graphene Passives on Flexible Substrates

Surya Abhishek Singaraju,\* Gabriel Cadilha Marques, Patric Gruber, Robert Kruk, Horst Hahn, Ben Breitung, and Jasmin Aghassi-Hagmann\*

Printed and flexible metal-oxide transistor technology has recently demonstrated great promise due to its high performance and robust mechanical stability. Herein, fully printed inverter structures using electrolyte-gated oxide transistors on a flexible polyimide (PI) substrate are discussed in detail. Conductive graphene ink is printed as the passive structures and interconnects. The additive printed transistors on PI substrates show an  $I_{on}/I_{off}$  ratio of  $10^6$  and show mobilities similar to the state-of-the-art printed transistors on rigid substrates. Printed meander structures of graphene are used as pull-up resistances in a transistor-resistor logic to create fully printed inverters. The printed and flexible inverters show a signal gain of 3.5 and a propagation delay of 30 ms. These printed inverters are able to withstand a tensile strain of 1.5% following more than 200 cycles of mechanical bending. The stability of the electrical direct current (DC) properties has been observed over a period of 5 weeks. These oxide transistor-based fully printed inverters are relevant for digital printing methods which could be implemented into roll-to-roll processes.

In recent times, flexible electronics is expanding into newer applications, enabled with many interconnected devices. To complement the smart back-end systems, technology development for the front-end devices has also received a fresh boost.<sup>[1]</sup> This includes the development of high-performance flexible electronics for applications such as memristors, radio-frequency identification devices, and displays.<sup>[2–4]</sup>


Concerning the semiconductor components in printed electronics, oxide materials offer high intrinsic mobilities and

environmental stability.<sup>[5]</sup> These are quite favorable for flexible electronics<sup>[6]</sup> and are printable because of the realization of cost effective and high-throughput solution-processed methods.<sup>[7]</sup> Examples include amorphous IGZO or crystalline  $\text{In}_2\text{O}_3$ .<sup>[8,9]</sup> Solution-processed and printed polycrystalline oxide transistors that can possibly be prepared on plastic substrates, are reported with greater device mobilities.<sup>[10,11]</sup> Subsequently, to date, there are noteworthy attempts to create printed oxide transistors and circuits using transistor-transistor logic (TTL) or transistor-resistor logic (TRL).<sup>[12–17]</sup> However, such works used deposition techniques such as photolithography, sputtering, or thermal evaporation to fabricate the electrodes and passive structures. These additional processes often result in defects on the surface of the substrate and in turn, obtain films of a poorer quality.

In addition, it would also limit the mechanical flexibility of the printed devices. Solution-processed methods, in contrast, offer conformity with the surface of flexible substrates, better flexibility, and digital-printing methods facilitate the integration of passive components into electronic circuits. Metallic inks such as silver- or carbon-based graphene oxide<sup>[18]</sup> and graphene nanoflake inks<sup>[19,20]</sup> are well tested as printed and flexible conductors and resistors. With regards to transistors, fully printed dielectric oxide transistors<sup>[21]</sup> and electrolyte-gated transistors (EGTs) using graphene inks for

S. A. Singaraju, G. C. Marques, Dr. R. Kruk, Prof. H. Hahn, Dr. B. Breitung, Prof. J. Aghassi-Hagmann  
Institute of Nanotechnology  
Karlsruhe Institute of Technology (KIT)  
Eggenstein-Leopoldshafen 76344, Germany  
E-mail: surya.singaraju@kit.edu; jasmin.aghassi@kit.edu

G. C. Marques  
Chair of Dependable Nano Computing (CDNC)  
Karlsruhe Institute of Technology  
Karlsruhe 76131, Germany

 The ORCID identification number(s) for the author(s) of this article can be found under <https://doi.org/10.1002/pssr.202000252>.

© 2020 The Authors. Published by WILEY-VCH Verlag GmbH & Co. KGaA, Weinheim. This is an open access article under the terms of the Creative Commons Attribution License, which permits use, distribution and reproduction in any medium, provided the original work is properly cited.

DOI: 10.1002/pssr.202000252

Dr. P. Gruber  
IAM-WBM Werkstoffmechanik 1 (WM1)  
Karlsruhe Institute of Technology  
Eggenstein-Leopoldshafen 76344, Germany

Prof. H. Hahn  
KIT-TUD Joint Research Laboratory Nanomaterials  
Institute of Materials Science  
Technische Universität Darmstadt  
Darmstadt D-64206, Germany

Dr. B. Breitung  
Karlsruhe Nano Micro Facility (KNMF)  
Karlsruhe Institute of Technology  
Eggenstein-Leopoldshafen 76344, Germany

Prof. J. Aghassi-Hagmann  
Department of Electrical Engineering  
Offenburg University of Applied Sciences  
Offenburg 77652, Germany

the passive components and an oxide semiconductor as the active component<sup>[22]</sup> were developed on rigid substrates. These exhibited low contact resistances and high device mobilities. Whereas, on flexible substrates, to date, there are limited studies on fully printed oxide electronics, as the processing of oxides on flexible substrates is rather undefined. Concerning printed oxides on flexible substrates, the macroscopic effects are influenced by the thicknesses, the elastic moduli, and the thermal expansion coefficients of the oxide film and the substrate.<sup>[23]</sup> The surface properties of the plastic substrate influence the wettability of the ink and morphology of the film.<sup>[24,25]</sup> In this work, the entire process of printing inverters in TRL on polyimide (PI) Kapton<sup>HN</sup> substrates using a precursor-based indium oxide ( $\text{In}_2\text{O}_3$ ) ink (processed at 350 °C) has been demonstrated.  $\text{In}_2\text{O}_3$  has been utilized as semiconductor in the EGTs for its high carrier concentration and hall mobility. The PI surface is modified using simple methods to facilitate the formation of smooth oxide films. Drop-on-demand deposition methods, for example, inkjet printing, are used to fabricate electronic circuits. Composite solid polymer electrolyte (CSPE) is used as the gating material, which allows low operational voltages. This is due to the formation of a electrical “double layer” that is typically a few nanometers in thickness. CSPE offers printability, low input voltage operation, conformal compatibility, and mechanical stability, and therefore, is very effective for use on flexible substrates. A top-gate is selected to be printed as opposed to a planar gate, to achieve faster switching speeds through reducing the gate-channel distance.<sup>[22]</sup> In TRL, a resistor load is used to “pull-up” low-input voltages to higher-output voltage. Graphene ink has been printed to create passive structures as well as the pull-up resistors. A comprehensive study

of the inverter signal gain ( $dV_{\text{OUT}}/dV_{\text{IN}}$ ), rise–fall times, and the propagation delay of the fully printed inverters are also computed. The characteristics of these fully printed inverters stand well with the state-of-the-art inverters printed on rigid substrates.

To obtain high-performance electronics, a dense and continuous oxide film is necessary. However, when the aqueous precursor of the  $\text{In}_2\text{O}_3$  is printed on the PI, a loss of the film uniformity due to the “coffee-ring effect” is observed in the oxide film (Figure S1a, Supporting Information). Moreover, the difference in the thermal expansion of indium oxide and the polymer substrate could form cracks in the oxide film during heating. To avoid this, the precursor is printed on a PI rinsed with a solution of 4:1 isopropanol and acetone (Figure 1a). This cleaning process aided in printing desired pattern with sharp edges implying that the rinsed PI surface has good wetting property. This can be confirmed from the sessile-goniometry studies that indicate a contact angle of 64.4° (Figure 1b), which falls in the range of most stable contact angle.<sup>[26]</sup> The precursor is then dried at 100 °C before annealing at 350 °C. Oxide films prepared in this way on the PI substrate have homogeneous morphology and can be seen clearly in an optical microscope (Figure S1b, Supporting Information). The dried film exhibited dense morphology even after annealing at 350 °C (Figure 1c). The surface profile of the oxide film is mapped using an atomic force micrograph and the roughness of the film is measured to be less than 5 nm.

The precursor ink for the channel, which is printed first, is dried at 100 °C. The passive electrodes are printed using graphene ink such that the channel has a width-to-length ratio ( $W/L$ ) of 60/150. The reason for using graphene ink is its high conductivity ( $22\,000\ \text{S m}^{-1}$ ) and low contact resistance with the

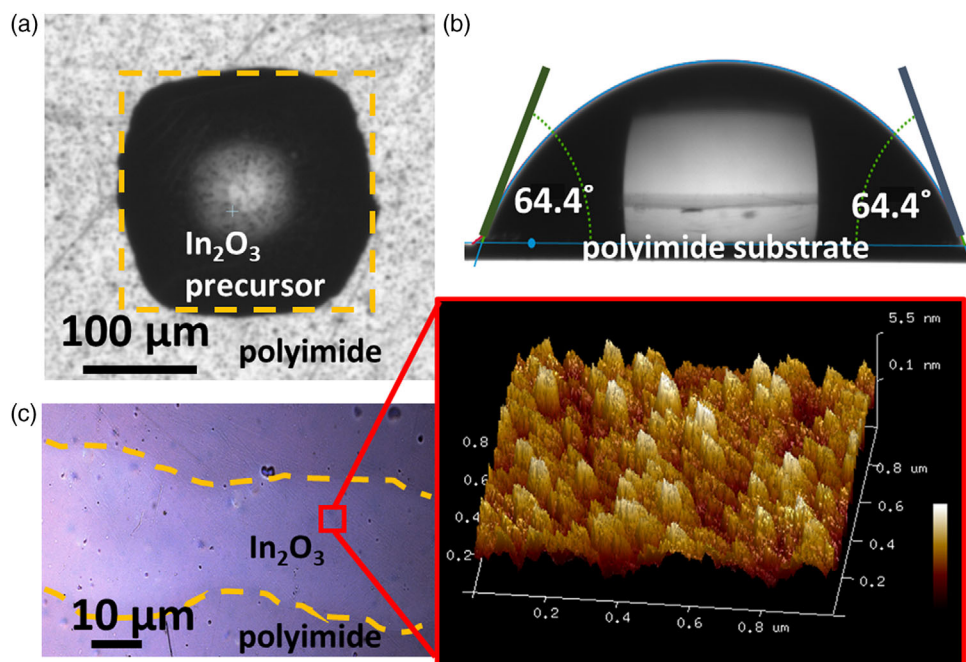


**Figure 1.** Printing and processing of highly smooth precursor-based indium oxide film on a clean PI substrate. a) Printed patterns that fit perfectly with the desired ones (as shown in yellow dashed lines) could be achieved. b) A contact angle of 64.4° is observed, indicating good wetting behavior of the clean PI. c) Optical image of the smooth and homogenous  $\text{In}_2\text{O}_3$  formed after the annealing step. In the inset, atomic force micrograph of 1  $\mu\text{m}^2$  area on the oxide film shows minimal roughness.

oxide in EGTs. In addition, graphene offers higher stability in presence of the electrolyte as compared with metallic inks like silver. Using silver gave rise to side reactions in the presence of a strong oxidizing agent like perchlorate. The precursor and the graphene passives are together annealed at 350 °C for 2 h to give rise to homogenous films of polycrystalline  $\text{In}_2\text{O}_3$  connected by conducting graphene electrodes. The resistance of the printed graphene ink is controlled by changing the length of the printed film and thus, meander structures of the graphene ink are printed at the drain electrode and processed at 250 °C to obtain a resistance of 250–400 k $\Omega$ . A detailed schematic of the printing of the inverters is shown in Figure S2, Supporting Information.

The fully printed transistors (Figure 2a,b) exhibit an off-current of about  $4 \times 10^{-11}$  and an on-current of  $2 \times 10^{-5}$  therefore displaying an on/off ratio of about  $10^6$ . Considerably negligible gate currents ( $10^{-9}$ ) indicate that the channel is isolated from the gate. The subthreshold slope in the linear region is 100 mV  $\text{dec}^{-1}$ . The threshold voltage, which is obtained through the extrapolation of the linear region of the  $I_{\text{DS}}$  versus  $V_{\text{GS}}$  plot at low drain-source voltage, is calculated to be 0.2 V. The hysteresis of the transistor threshold voltages in the forward and reverse sweeps of the transfer curve ( $V_{\text{th,forward}} - V_{\text{th,backward}}$ ) carries a value of 0.15 V. This is because the current density inhomogeneities due to electrode roughness and low ionic

mobility leads to high resistance and slow response of ions at the electrode/electrolyte interface at the given input voltages.<sup>[27]</sup> The device mobility is extracted from the linear region of the transfer curve (Figure 2a), using the following transconductance equation (Equation (1))

$$\mu C_{\text{DL}} = \frac{Lg_m}{WV_{\text{DS}}}, \quad |V_{\text{DS}}| \ll |V_{\text{GS}} - V_{\text{Th}}| \quad (1)$$

where  $L$  is the length of the channel,  $W$  the width,  $V_{\text{DS}}$  the drain potential,  $g_m$  the transconductance value ( $dI_{\text{DS}}/dV_{\text{GS}}$ ), and  $C_{\text{DL}}$  the double layer capacitance. The  $\mu C_{\text{DL}}$  is 400  $\mu\text{F V}^{-1}\text{s}^{-1}$  for the printed transistor. Considering the capacitance value of 35  $\mu\text{F cm}^{-2}$  as calculated using cyclic voltammetry,<sup>[22]</sup> the device mobility ( $\mu$ ) is 12  $\text{cm}^2 \text{V}^{-1}\text{s}^{-1}$ . This value is similar to the fully printed transistors that are printed on rigid substrates such as glass.

In the printed inverter, as the n-type EGT is in off-state at low input voltages, the output voltage can be “pulled-up” to the supply voltage,  $V_{\text{DD}}$ . To facilitate this, a graphene resistor load of 250–400 k $\Omega$  is printed in series with the transistor (TRL inverter). Graphene ink offers higher resistance compared with metallic inks like silver and hence, desired high load resistance values in a TRL can be printed more easily using less area. As the resistance of the printed graphene increases linearly with the length

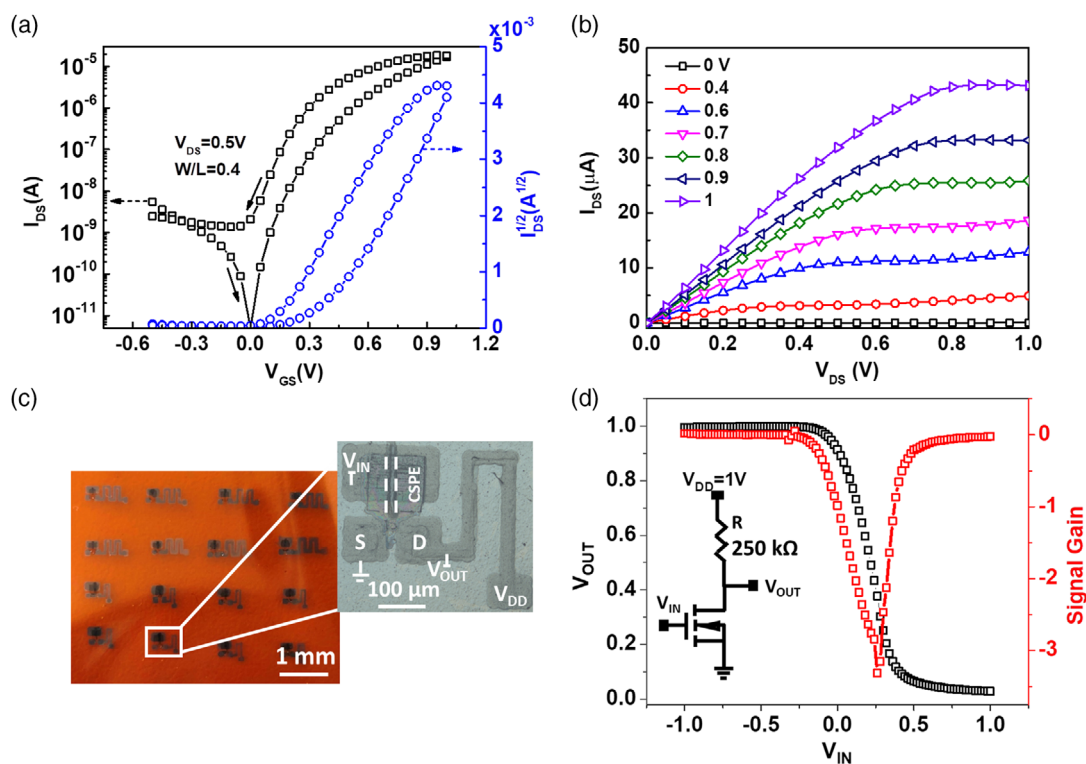


**Figure 2.** Fully printed EGT and inverter on flexible PI substrate. a) Transfer characteristics of a typical fully printed electrolyte-gated oxide transistor on a flexible substrate. The applied drain voltage is 0.5 V. The squares represent  $I_{\text{DS}}$  versus  $V_{\text{GS}}$ , whereas the circles represent  $I_{\text{DS}}^{1/2}$  versus  $V_{\text{GS}}$ . The threshold voltage is calculated to be 0.2 V. b)  $I_{\text{DS}}-V_{\text{DS}}$  output characteristics of the transistor with  $V_{\text{GS}}$  varied from 0 to 1 V. c) Microscope image of the fully printed inverters prepared using TRL. The inset shows an image of a single inverter with the source (S), drain (D) electrodes, pull-up resistor to the right, the CSPE and top-gate between the dashed lines. Source is grounded. d) The DC characteristics of the printed inverter. The schematic of the inverter circuit is shown in the inset. The calculated peak signal gain is 3.5.

of the structure (Figure S3, Supporting Information), line with a length of 1000  $\mu\text{m}$ , a constant width of 75  $\mu\text{m}$ , and a thickness of 300 nm are printed (Figure 2c) to obtain the 250 k $\Omega$  resistance load in the inverter. The direct current (DC) characteristics of the printed inverter for a supply voltage ( $V_{\text{DD}}$ ) of 1 V given at the resistor load and an input voltage ( $V_{\text{IN}}$ ) swept from  $-1$  to 1 V at the gate, are shown in Figure 2d. Output voltage ( $V_{\text{OUT}}$ ) of 0.99 and 0.03 V at low and high  $V_{\text{IN}}$ , respectively, are observed. The  $V_{\text{OUT}}$  did not reach a minimum of 0 V as expected, as the transistor carries some resistance even when the channel has been formed fully. The maximum signal gain,  $dV_{\text{OUT}}/dV_{\text{IN}}$ , is 3.5 (Figure 2d), with a switching threshold potential ( $V_{\text{IN}} = V_{\text{OUT}}$ ) of 0.25 V. The device performance in this study is similar to the reported values that use lithography processes to fabricate circuits in TRL.<sup>[16]</sup> As every component of the inverter is printed, certain nonuniformities need to be accounted for. Therefore, we demonstrate the reproducibility by fully printing ten inverters of matching dimensions (Figure S4, Supporting Information). The inverters function at switching thresholds between 250 and 400 mV and exhibit a signal gain between 2.5 and 3.5.

The transient properties of the inverter at a frequency of 1 Hz are measured, as shown in Figure 3. The fall time ( $t_{\text{fall}}$ ) from 90% to 10% of the output values and the rise time ( $t_{\text{rise}}$ ) from 10% to 90% of the output value are calculated between 1 and 2 s. The rise and fall times are 100 and 120 ms, respectively. The noise margins measured from a  $-1$  slope in the DC characteristics are calculated to be 140 mV in the high-level ( $\text{NM}_{\text{H}}$ ) region and 50 mV in the low-level ( $\text{NM}_{\text{L}}$ ) region. The propagation delay calculated as a difference between 50% of input and output curves amounts to 30 ms for the fully printed inverters. Although the inverter performance could be technologically improved, it is still potentially suitable for fully printed sensing applications such as, blood glucose level monitoring, temperature, gas sensing, and so on.

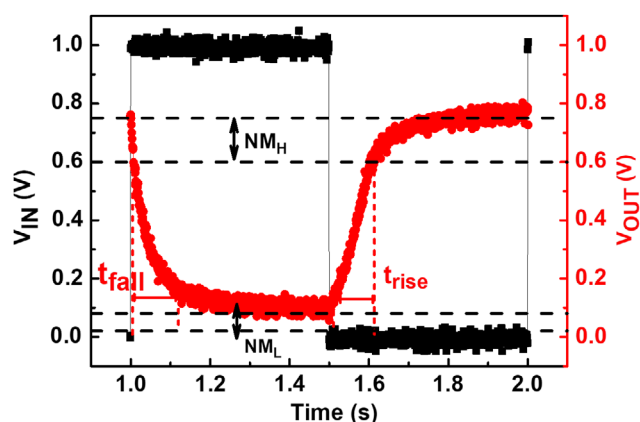


**Figure 3.** The transient properties of the printed inverter on flexible substrate at 1 Hz. Fall ( $t_{\text{fall}}$ ) and rise ( $t_{\text{rise}}$ ) in a time period of 1 s (vertical red dotted lines) are calculated from 90% and 10% of the  $V_{\text{OUT}}$ . The  $V_{\text{IN}}$  is pulsed from 0 to 1 V and  $V_{\text{DD}}$  is 1 V (black rectangular pulses). The noise margins for the high and low levels are depicted by the horizontal black dotted lines. These are calculated from slope of  $-1$  on the  $dV_{\text{OUT}}/dV_{\text{IN}}$  DC response.

The mechanical stability of the devices was determined by performing bending and elongation tests to measure the tensile strain on the devices, as shown by Equation (2). The thickness of the PI substrate ( $\epsilon_{\text{sub}}$ ) is 125  $\mu\text{m}$  and the thickness of the oxide semiconductor ( $t_{\text{ox}}$ ) is 200 nm. The devices consisting of printed graphene and the oxide film adhere very well to the PI, and therefore, the tensile tests on the PI directly affect the inverters. Mechanical bending in a radius ( $r$ ) of 4.5 mm, which is suitable for flexible applications such as wearable electronics. The bending resulted in a tensile strain of 1.5%. Complementary to the bending tests, elongation tests on the oxide film were conducted as well. The film begins to crack slightly, on an applied strain of greater than 1.5% (Figure S5, Supporting Information). It should be noted that the graphene electrodes and resistors show no sign of cracks and remain intact even more than an applied tensile strain of 8%.

$$\text{Strain} = \frac{\epsilon_{\text{sub}} + t_{\text{ox}}}{2r} \quad (2)$$

The printed, flexible devices were subjected to bending tests of more than 200 cycles at a radius of 4.5 mm, and the relevant parameters were measured. The inverter gain normalized with the initial gain of 3.5 ( $A_{V_0}$ ) is shown in Figure 4 and remained largely constant throughout 200 cycles of mechanical bending. Stability of the inverters over 4 weeks are conducted as well, to determine the lifetime of the inverters (inset, Figure 4). The propagation delay remains constant throughout as observed in the transient properties (Figure S6, Supporting Information). The DC characteristics of the printed inverters measured over 4 weeks indicate a shift of the slope but with no significant trend. This can be attributed to the variations in contact resistance that differ with each new measurement. This could also be due to the inconsistent shift in the threshold voltage of the printed transistors<sup>[28]</sup> with time as the ion mobility in the electrolyte gets affected with drying. For better understanding, the performance of the printed and flexible inverters in this work, a comparison

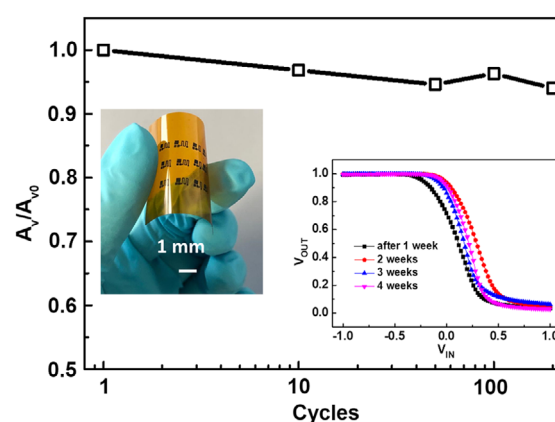


**Figure 4.** The mechanical and temporal stabilities of the printed oxide transistors. The signal gain of the inverters normalized with the initial value remained constant over 200 bending cycles. In the inset, to the left, is an image of the devices on the flexible substrate before printing the electrolyte. The oxide film withstands a tensile strain of 1.5%. Inset graph shows the stability of the printed inverters as a function of time, measured over 4 weeks throughout which, the signal gain remained constant.



**Table 1.** Comparison of results of this work with literature results.

Material	Substrate	Fabrication	Logic	Signal gain	Delay [ms]	Ref.
TIPS-Pentacene <sup>a)</sup>	Arylite	Ink-jet printing	TTL	5.5	0.44	[29]
sc-SWCNT <sup>b)</sup>	PET	Atomic layer deposition, lithography, printing	TTL	33	0.06	[30]
TIPS-Pentacene <sup>a)</sup>	Polycarbonate	Screen printing, slot casting	TTL	9	NA	[31]
In <sub>2</sub> O <sub>3</sub>	Glass	Lithography, ink-jet printing	TTL	21	NA	[10]
ZnO	Flexible SiO <sub>2</sub>	Lithography, doctor blading	TTL	21	0.06	[17]
In <sub>2</sub> O <sub>3</sub>	Glass	Lithography, ink-jet printing	TRL	4	2.3	[32]
In <sub>2</sub> O <sub>3</sub>	Kapton <sup>HN</sup>	Ink-jet printing, microplotting	TRL	3.5	30	This work

<sup>a)</sup>TIPS-Pentacene: 6,13-Bis(triisopropylsilylethynyl)pentacene; <sup>b)</sup>sc-SWCNT: semiconducting single-walled carbon nanotubes.

with state-of-the-art printed inverter logics is shown in **Table 1**. Quite evidently, the device in this work stands out as the only example of fully printed oxide inverter. However, the parameters such as gain and delay can further be improved by more controlled printing or prestructuring and using a TTL with n-and p-type devices.

In summary, fully printed oxide-based inverters in TRL have been fabricated on flexible PI substrate. The lithography process used in the state-of-the-art methods is replaced by direct printing, which simplifies the fabrication of passive structures on polymer substrates. The printed flexible transistors exhibited a threshold voltage of 0.2 V and  $I_{on}/I_{off}$  value of 10<sup>6</sup>. A resistor load of 250–400 k $\Omega$  is printed to fabricate the TRL gate in form of an inverter. A signal gain of 3.5 and a propagation delay of 30 ms is observed for the printed, flexible inverters while exhibiting decent mechanical endurance and temporal stability. The propagation delay can be further improved by more controlled device dimensions and architecture and increasing the conductivity of the printed graphene passive electrodes. Considering the drop-on-demand printing techniques used in this study, this can be advanced into high-throughput digital fabrication of printed and flexible electronics.

## Experimental Section

**Preparation of the Inks:** PI Kapton<sup>HN</sup> was utilized for its excellent thermal and mechanical properties, coupled with an observed chemical stability with the printed inks. The PI was preheated to 400 °C to enable a uniform processing of the subsequently printed semiconductor. The n-type indium oxide semiconductor was synthesized using the precursor route in which, 0.05 M of In(NO<sub>3</sub>)<sub>3</sub>·xH<sub>2</sub>O (99.99%, Sigma-Aldrich) was dissolved in a 4:1 mixture of deionized H<sub>2</sub>O and Glycerol. The solution was continuously stirred for an hour to obtain a clear solution and filtered, first through a 0.45 and then a 0.2  $\mu$ m polyvinylidene fluoride (PVDF) filter. The source and drain electrodes were printed using a commercially available graphene ink (Sigma-Aldrich). The ink consisted of graphene flakes (0.2–3  $\mu$ m) stabilized by ethyl cellulose in cyclohexanone and terpeneol.

To prepare the CSPE, the following recipe is used. About 0.3 g of poly(vinyl alcohol) (PVA, average MW = 13–23 kDa, 98% hydrolyzed, Sigma-Aldrich) was added to 6 g of dimethyl sulfoxide (DMSO, anhydrous 99.9%, Sigma-Aldrich) solvent and was stirred continuously at 85 °C for 1 h until the PVA was completely dissolved. Another solution was prepared by adding 0.07 g lithium perchlorate (LiClO<sub>4</sub>, anhydrous, 98%, Alfa Aesar) in 0.63 g propylene carbonate (PC, anhydrous, 99.7%, Sigma-Aldrich) plasticizer and stirred continuously for 1 h. The two solutions were then mixed

together and stirred at room temperature overnight to obtain the CSPE. The CSPE was then filtered through a 0.2  $\mu$ m polytetrafluoroethylene (PTFE) filter. The top-gated electrode was printed using a commercially available poly(3,4 ethylene-dioxythiophene) poly(styrenesulfonate) (PEDOT:PSS) ink (0.8% in H<sub>2</sub>O, Sigma-Aldrich).

**Fabrication and Characterization:** The PI substrate was initially preheated to 400 °C. On surface modification, the indium oxide precursor was printed onto the substrate using a Dimatix 2831 ink-jet printer and was then dried at 100 °C. Graphene ink for the passive electrodes was printed using a Sonoplot microplotter as the graphene, due to its flake size and agglomeration lead to the clogging of the ink-jet printer nozzles. The precursor and the graphene passive structures were then annealed at 350 °C for 2 h. A meander-shaped resistor attached to the drain was then printed using the graphene ink and heated to 250 °C. Subsequently, CSPE and PEDOT:PSS were ink-jet printed as the gating material and the top-gate, respectively. A detailed flowchart of the device preparation is shown in Figure S5, Supporting Information. The contact angle of the precursor ink on the PI substrate were measured using sessile-drop goniometry (DSA-30, KRÜSS). The printed transistors and inverters were then electrically characterized using an Agilent 4156C semiconductor analyser for the DC characteristics. Furthermore, the transient characteristics were observed using a Keithley 267 and a Tektronix TDS3000C Digital Oscilloscope.

The mechanical flexibility of the devices was tested using a 5 mm steel rod, and the tensile strength of the printed films was tested using an in-house developed mechanical tester unit.

## Supporting Information

Supporting Information is available from the Wiley Online Library or from the author.

## Acknowledgements

S.A.S. would like to thank Dr. Julia Smuth at the Institute for Functional Interfaces, KIT for her help and discussion on contact angle measurements and Daisy Agrawal (University of Waterloo) for assistance in the work. S.A.S. acknowledges the Ministry of Science, Research and Arts of the state of Baden Württemberg for funding research through the MERAGEM graduate school. B.B. and H.H. appreciate the support of EnABLES, a project funded by the European Unions Horizon 2020 research and innovation program under grant agreement no. 730957. Financial support by the German Research Foundation (to D.B., grant no. BR 3499/5-1) is gratefully acknowledged. All authors acknowledge support given by the KIT-Publication Fund of the Karlsruhe Institute of Technology.

## Conflict of Interest

The authors declare no conflict of interest.

## Keywords

flexible devices, fully printed devices, inverters, metal-oxide transistors, printed graphene, tensile strength

Received: May 16, 2020

Revised: June 10, 2020

Published online: June 30, 2020

- 
- [1] S. F. Jilani, A. Rahimian, Y. Alfadhl, A. Alomainy, *Flexible Printed Electron.* **2018**, 3, 035003.
- [2] W. Zhang, Y. Mao, W. Duan, *Phys. Status Solidi RRL* **2019**, 13, 1900016.
- [3] Y. Wang, C. Yan, S.-Y. Cheng, Z.-Q. Xu, X. Sun, Y.-H. Xu, J.-J. Chen, Z. Jiang, K. Liang, Z.-S. Feng, *Adv. Funct. Mater.* **2019**, 29, 1902579.
- [4] K. R. Sarma, in *Handbook of Visual Display Technology*, Springer, Berlin, Heidelberg **2016**, pp. 1–12.
- [5] E. Fortunato, P. Barquinha, R. Martins, *Adv. Mater.* **2012**, 24, 2945.
- [6] P. Xiao, T. Dong, L. Lan, Z. Lin, W. Song, E. Song, S. Sun, Y. Li, P. Gao, D. Luo, M. Xu, J. Peng, *Phys. Status Solidi RRL* **2016**, 10, 493.
- [7] L. Petti, N. Mzenrieder, C. Vogt, H. Faber, L. Bthe, G. Cantarella, F. Bottacchi, T. D. Anthopoulos, G. Trster, *Appl. Phys. Rev.* **2016**, 3, 021303.
- [8] P. Barquinha, R. Martins, L. Pereira, E. Fortunato, *Transparent Oxide Electronics*, John Wiley & Sons, Ltd, Chichester, UK **2012**.
- [9] R. Chen, L. Lan, *Nanotechnology* **2019**, 30, 312001.
- [10] S. K. Garlapati, G. C. Marques, J. S. Gebauer, S. Dehm, M. Bruns, M. Winterer, M. B. Tahoori, J. Aghassi-Hagmann, H. Hahn, S. Dasgupta, *Nanotechnology* **2018**, 29, 235205.
- [11] M.-G. Kim, M. G. Kanatzidis, A. Facchetti, T. J. Marks, *Nat. Mater.* **2011**, 10, 382.
- [12] S. K. Garlapati, T. T. Baby, S. Dehm, M. Hammad, V. S. K. Chakravadhanula, R. Kruk, H. Hahn, S. Dasgupta, *Small* **2015**, 11, 3591.
- [13] K. J. Yu, Z. Yan, M. Han, J. A. Rogers, *npj Flexible Electron.* **2017**, 1, 1.
- [14] J. Leppniemi, K. Eiroma, H. Majumdar, A. Alastalo, *ACS Appl. Mater. Interfaces* **2017**, 9, 8774.
- [15] N. Yamada, R. Ino, H. Tomura, Y. Kondo, Y. Ninomiya, *Adv. Electron. Mater.* **2017**, 3, 1700298.
- [16] G. C. Marques, D. Weller, A. T. Erozan, X. Feng, M. Tahoori, J. Aghassi-Hagmann, *Adv. Mater.* **2019**, 31, 1806483.
- [17] F. Z. Bidoky, B. Tang, R. Ma, K. S. Jochem, W. J. Hyun, D. Song, S. J. Koester, T. P. Lodge, C. D. Frisbie, *Adv. Funct. Mater.* **2019**, 30, 1902028.
- [18] W. Yang, C. Wang, *J. Mater. Chem. C* **2016**, 4, 7193.
- [19] E. B. Secor, T. Z. Gao, A. E. Islam, R. Rao, S. G. Wallace, J. Zhu, K. W. Putz, B. Maruyama, M. C. Hersam, *Chem. Mater.* **2017**, 29, 2332.
- [20] D. Song, A. Mahajan, E. B. Secor, M. C. Hersam, L. F. Francis, C. D. Frisbie, *ACS Nano* **2017**, 11, 7431.
- [21] W. J. Scheideler, R. Kumar, A. R. Zeumault, V. Subramanian, *Adv. Funct. Mater.* **2017**, 27, 1606062.
- [22] S. A. Singaraju, T. T. Baby, F. Neuper, R. Kruk, J. A. Hagmann, H. Hahn, B. Breitung, *ACS Appl. Electron. Mater.* **2019**, 1, 1538.
- [23] J. C. Grosskreutz, *J. Electrochem. Soc.* **1969**, 116, 1232.
- [24] L. Nayak, S. Mohanty, S. K. Nayak, A. Ramadoss, *J. Mater. Chem. C* **2019**, 7, 8771.
- [25] F. Shao, Q. Wan, *J. Phys. D: Appl. Phys.* **2019**, 52, 143002.
- [26] *Surface Science Techniques*, (Eds: G. Bracco, B. Holst), Springer, Berlin, Heidelberg **2013**.
- [27] S. H. Kim, K. Hong, W. Xie, K. H. Lee, S. Zhang, T. P. Lodge, C. D. Frisbie, *Adv. Mater.* **2012**, 25, 1822.
- [28] B. Nasr, D. Wang, R. Kruk, H. Rsner, H. Hahn, S. Dasgupta, *Adv. Funct. Mater.* **2012**, 23, 1750.
- [29] S. Chung, J. Ha, Y. Hong, *Flexible Printed Electron.* **2016**, 1, 045003.
- [30] W. Xu, Z. Liu, J. Zhao, W. Xu, W. Gu, X. Zhang, L. Qian, Z. Cui, *Nanoscale* **2014**, 6, 14891.
- [31] J. Chang, X. Zhang, T. Ge, J. Zhou, *Org. Electron.* **2014**, 15, 701.
- [32] G. C. Marques, S. K. Garlapati, S. Dehm, S. Dasgupta, H. Hahn, M. Tahoori, J. Aghassi-Hagmann, *Appl. Phys. Lett.* **2017**, 111, 102103.